The Spine Journal 18 (2018) 472–481

Clinical Study

The mechanism of thoracolumbar burst fracture may be related to the basivertebral foramen

Xuyang Zhang, MD[a,1], Shengyun Li, MD[a,1], Xing Zhao, MD[a], Blaine A. Christiansen, MD, PhD[b], Jian Chen, PhD[a], Shunwu Fan, MD[a], Fengdong Zhao, MD, PhD[a,*]

[a]*Department of Orthopaedics, Sir Run Run Shaw Hospital, School of Medicine, Zhejiang University, No. 3, Qingchun Rd East, Hangzhou 310016, China*
[b]*Department of Orthopaedic Surgery, UC Davis Medical Center, 4635 2nd Ave, Suite 2000, Sacramento, CA 95817, USA*

Received 21 February 2017; revised 4 August 2017; accepted 9 August 2017

Abstract

BACKGROUND CONTEXT: The basivertebral foramen (BF), located in the middle posterior wall of the vertebral body, may induce local weakness and contribute to the formation of a retropulsed bone fragment (RBF) in thoracolumbar burst fracture (TLBF). We hypothesize that the mechanism of TLBF is related to the BF.

PURPOSE: This study aimed to clarify the relationship between RBFs and the BF in TLBFs, and to explain the results using biomechanical experiments and micro-computed tomography (micro-CT).

STUDY DESIGN: A comprehensive research involving clinical radiology, micro-CT, and biomechanical experiments on cadaveric spines was carried out.

PATIENT SAMPLE: A total of 162 consecutive patients diagnosed with TLBF with RBFs, drawn from 256 patients who had reported accidents or injuries to their thoracolumbar spine, comprised the patient sample.

OUTCOME MEASURES: Dimensions and location of the RBFs in relation to the BF were the outcome measures.

MATERIALS AND METHODS: Computed tomography reconstruction imaging was used to measure the dimensions and location of RBFs in 162 patients (length, height, width of RBF and vertebral body). Furthermore, micro-CT scans were obtained of 10 cadaveric spines. Each vertebral body was divided into three layers (superior, middle, and inferior), and each layer was divided further into nine regions (R1–R9). Microarchitecture parameters were calculated from micro-CT scans, including bone volume fraction (BV/TV), connectivity (Conn.D), trabecular number (Tb.N), trabecular thickness (Tb.Th), and bone mineral density (BMD). Differences were analyzed between regions and layers. Burst fractures were simulated on cadaveric spines to explore the fracture line location and test the relationship between RBFs and BF.

RESULTS: Retropulsed bone fragment width was usually one-third of the width of the vertebral body, whereas RBF length and height were approximately half of the corresponding vertebral body dimensions. Measures of trabecular bone quality were generally lowest in those central and

FDA device/drug status: Not applicable.

Author disclosures: ***XuZ:*** Grant: National Natural Science Foundation of China (No. 31270997 and No. 81672208) (E, Paid directly to institution/employer), pertaining to the submitted work. ***SL:*** Grant: National Natural Science Foundation of China (No. 31270997 and No. 81672208) (E, Paid directly to institution/employer), pertaining to the submitted work. ***XiZ:*** Grant: National Natural Science Foundation of China (No. 31270997 and No. 81672208) (E, Paid directly to institution/employer), pertaining to the submitted work. ***BAC:*** Grant: National Natural Science Foundation of China (No. 31270997 and No. 81672208) (E, Paid directly to institution/employer), pertaining to the submitted work. ***SF:*** Grant: National Natural Science Foundation of China (No. 31270997 and No. 81672208) (E, Paid directly to institution/employer), pertaining to the submitted work. ***FZ:*** Grant: National Natural Science Foundation of China (No. 31270997 and No. 81672208) (E, Paid directly to institution/employer), pertaining to the submitted work. ***JC:*** Grant: National Natural Science Foundation of China (No. 31270997 and No. 81672208) (E, Paid directly to institution/employer), pertaining to the submitted work.

The disclosure key can be found on the Table of Contents and at www.TheSpineJournalOnline.com.

This study was partially supported by the National Natural Science Foundation of China (No. 31270997 and No. 81672208).

* Corresponding author. Department of Orthopaedics, Sir Run Run Shaw Hospital, School of Medicine, Zhejiang University, No. 3, Qingchun Rd East, Hangzhou 310016, China. Tel.: 0086-13858120759; fax: 0086-571-86044817.

E-mail address: zhaodong68@hotmail.com (F. Zhao)

[1] Xuyang Zhang and Shengyun Li contributed equally to this work.

https://doi.org/10.1016/j.spinee.2017.08.237

superior regions of the vertebral body which are adjacent to the BF and which are most affected by burst fracture. In simulated TLBFs, the fracture line went across the vertex or upper surface of the BF. **CONCLUSIONS:** The most vulnerable regions in the vertebral body lie within or just superior to the BF. The central MR2 region in particular is at risk of fracture and RBF formation.

Keywords: Basivertebral foramen; Biomechanical experiment; Microarchitecture; Retropulsed bone fragment; Thoracolumbar burst fracture; Vertebral body

Introduction

Approximately 50,000 traumatic injuries resulting in fractures of the bony spinal column occur annually in the United States [1–3]. Nearly 90% of all spinal fractures occur in the thoracolumbar region, and thoracolumbar burst fractures (TLBF) comprise 10%–20% of such injuries [1,2,4]. Common imaging features include anterior vertebral height loss, discontinuity in the posterior cortex, kyphosis deformity, vertebral fracture, and spinal stenosis [1,5,6]. Retropulsed bone fragments (RBFs) appear to characterize TLBFs. They are often located on the posterior upper margin of vertebrae, especially when flexion injury is combined with compression force [7]. The costs of these injuries to individuals and societies are great, especially when they are accompanied by spinal cord injuries [8]. These fragments are of great significance in estimating nerve injury, vertebral canal occlusion, fracture stability, and posterior longitudinal ligament rupture [5,6,9,10]. Also, choice of surgical approach may benefit from an understanding of the mechanism of RBFs according to the load-sharing scoring system [11].

By measuring the deformation of different areas of vertebrae, Hongo et al. concluded that stresses are concentrated near the bases of the pedicles [12], and this was supported by Qiu et al. using finite element modeling [13]. Compression fractures are more likely to occur in the posterior superior areas of the vertebral body which are shielded by the posterior column and so have less trabecular bone [14]. Heggeness et al. observed internal trabecular structure, and suggested that trabeculae radiate from the medial part of the pedicles so that the vertebral body cortex close to the base of the pedicles becomes thin [15]. Hence the pedicles may form the left and right boundaries of RBFs. As considered by Langrana et al., the vertical load breaks the vertebral end plate and presses the intervertebral disc into vertebral body, increasing its pressure until it bursts [1]. At the same time it causes the basal area of the pedicles to fracture and lead to the formation of an RBF [2,16]. However, this can hardly explain why the lower boundary of the fracture fragment is always located in the middle part of the vertebral body. By measuring the strength of the different areas of the vertebral end plate, Zhao et al. [17] found that when vertebrae are compressed naturally by adjacent intervertebral discs, cranial end plates usually fail before caudal end plates because they are thinner and supported by less dense trabecular bone. This can explain why fracture more often happens near the upper end plate.

We have observed that RBFs are often located above the basivertebral foramen (BF) which lies in the posterior wall of the vertebral body, in the median sagittal plane between the two pedicles. It provides a pathway for blood vessels to enter the vertebral body [17–19] (Fig. 1) and may induce local weakness in the posterior vertebral wall, leading to excessive stress concentrations [7]. We have also observed that many RBFs include all or part of the upper surface of the BF, suggesting that it may be a potential risk in thoracolumbar fracture involving an RBF.

Our study aims to explore whether the BF affects the distribution of vertebral trabecular microarchitecture and strength, and characterize its relationship with RBFs. Accordingly, we measured RBFs in computed tomography (CT) construction images to determine the specific location of RBFs and their proximity to the BF. We also analyzed regional trabecular bone variations using micro-CT scanning to find out where the bone is weakest. In addition, we simulated burst fractures on cadaveric specimens and analyzed the character of simulated RBFs to validate our conjecture (Fig. 2).

Materials and methods

Study sample

Patients or their family members agreed to our study, and signed the informed consents. The study was reviewed and approved by the institutional review board and the ethics

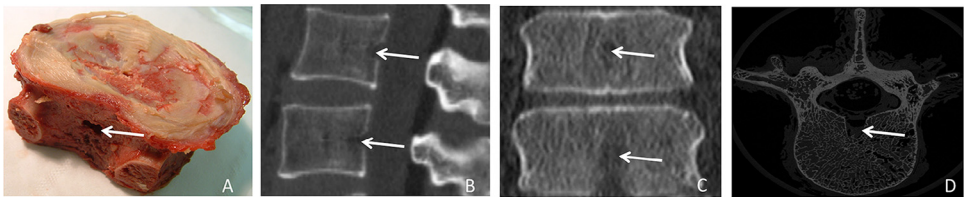

Fig. 1. The location of the basivertebral foramen in the posterior wall of the vertebral body is indicated by arrows: (A) cadaveric specimen, (B) CT sagittal plane image, (C) CT coronal plane image, and (D) micro-CT transverse plane image of vertebra.

EVIDENCE & METHODS

Context
In this radiographic and biomechanical study, the authors aimed to assess a potential role of the basivertebral foramen in the formation and propagation of the retropulsed fragment in burst fractures.

Contribution
They found that bone was of lesser biomechanical quality in the region of the foramen: the fracture lines run in this region and suggest that this could be a contributing factor to fragment occurrence.

Implications
The study provides some insight. Criticisms might include whether more upstream biomechanical phenomena (the endplate failure as an example) might not "decide" how the rest of it fatefully fails regardless of more downstream effects of small foramen that happen to be in the way, or whether the study is strictly of academic interest (in that no clinical application is likely) and, thus, better use of potentially scarce cadaveric specimens and brainpower may have been considered.

committee of the authors' institution. We retrospectively reviewed 256 patients who had reported accidents or injuries to their thoracolumbar spine between January 2013 and December 2016, and for whom we had dual-energy X-ray absorptiometry (DXA), radiographs, CT, and magnetic resonance imaging (MRI). Those patients diagnosed with TLBF with an RBF were chosen as the Fracture Group. Patients diagnosed with compression fracture, tumor, tuberculosis, or vertebral deformation were excluded according to the results of radiology [7]. The Fracture Group comprised 37 patients with T12 burst fracture,76 patients with L1 burst fracture, and 49 patients with L2 burst fracture. Of these 162 patients, 97 were men (age range 18–46 years, mean (STD) 35 (13) years) and 65 were women (age range 24–42 years, mean (STD) 32 (17) years).

CT imaging

Unenhanced CT was undertaken with the use of a 16-channel MDCT (Sensation 16; Siemens, Somatom, Forchheim, Germany) from Thoracic 11 to Lumbar 3. The following parameters were used: 120 kV, 115 mAs fixed tube current, pitch 0.9, gantry rotation time 1 seconds. Sagittal images were reconstructed with a 1-mm section thickness at 1-mm section intervals and an approximate 20×20-cm field of view, respectively. Images were displayed on a picture archiving and communications system, usually with a 1,500-HU window width and 500-HU window center.

Parameter measurement of retropulsed bone fragment (RBF)

CT transverse images and sagittal reconstruction images were obtained. In transverse images, the length of the RBF (RL) and the length of the vertebral body (VL) were measured. In sagittal reconstruction images, various dimensions were also measured at the fracture level, including the width of the RBF (RW), width of the vertebral body (VW), the height of the RBF (RH), and the height of the vertebral body (VH) (Fig. 3).

Parameters were independently measured three times by an experienced radiologist and by a senior orthopedic surgeon, who were blinded to patient information. Each measurement was made three times and averaged. The proportions RL/VL, RW/VW, and RH/VH were calculated.

Cadaveric material and specimen preparation

We collected 12 fresh-frozen human lumbar spines (T12–L2) from donors. Spine specimens were immersed in normal saline for DXA, radiographs, CT, and MRI. Specimens from donors who had suffered tumor, trauma, tuberculosis, and vertebral deformation were excluded according to the results of DXA, CT, and MRI. Of the 10 retained specimens, 6 were men (age range 38–68 years, mean (STD) 51±9 years), and 4 were women (age range 41–72 years, mean (STD) 56±11 years). After routine imaging examination, we divided each specimen into three vertebral bodies (T12, L1, and L2) which

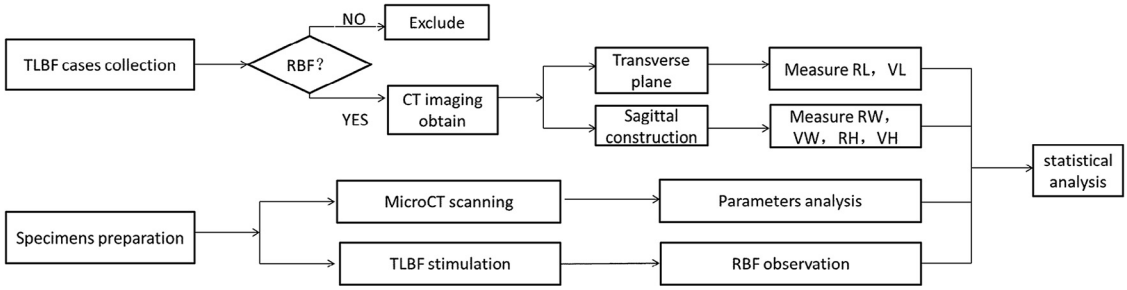

Fig. 2. Experimental design. TLBF, thoracolumbar burst fracture; RBF, retropulsed bone fragment; RL, length of retropulsed bone fragment; VL, length of vertebrae; RW, width of retropulsed bone fragment; VW=the width of vertebrae; RH, the height of retropulsed bone fragment; VH, the height of vertebrae.

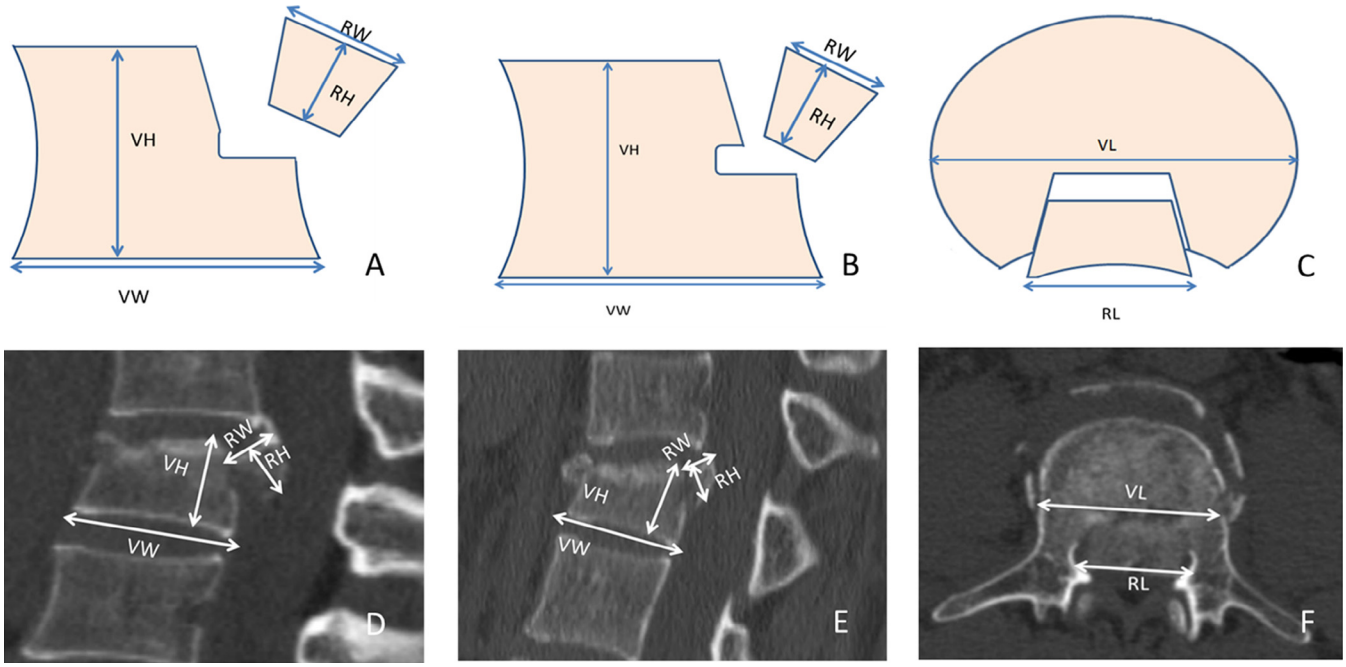

Fig. 3. Parameter measurement of RBF. In the transverse plane image, RL is the distance from the left corner to the right corner of the fracture. VL is the maximum length of vertebral body (A, D). In CT sagittal reconstruction image, RW is the distance between posterior corner of cranial end plate and perpendicular from the anterior inferior corner of RBF to the cranial end plate. VW is the maximum width of vertebral body. RH is the vertical distance from the vertex to the cranial end plate. VH is the maximum height of vertebral body (B, C, E, F). The fracture line of RBF goes across the vertex of BF (B, E). The fracture line of RBF goes across the upper surface of BF (A, D). RBF, retropulsed bone fragment; BF, basivertebral foramen; CT, computed tomography.

were stored in sealed bags at −20°C for micro-CT scanning [20].

Micro-CT scanning

Before scanning, vertebral body specimens were thawed and soaked in normal saline. Then they were successively placed in a micro-CT scanner (μCT100, Scanco Medical AG, Brüttisellen, Switzerland), where they were aligned along the *x*-axis of the scanner, and scanned at a nominal spatial resolution of 49.2 μm (field of view 90.1 mm, 1,834×1,834 pixels). The scanning parameters were 70 kVp, 200 μA, and 300 ms integration time. The following microstructural parameters of vertebral trabecular bone (without cortical components) were obtained through three-dimensional morphometric analysis [21]: bone volume fraction (BV/TV), bone mineral density (BMD), connectivity density (Conn.D), trabecular number (Tb.N), trabecular thickness (Tb.Th), trabecular spacing (Tb.Sp), and structure model index (SMI).

Micro-CT imaging assessment

Three-dimensional reconstruction images of the superior, middle (containing the BF), and inferior one-third of each vertebral body were obtained. Each layer was divided into nine equal regions for analysis (Fig. 4). Superior, middle, and inferior regions were labeled as SR1–SR9, MR1–MR9, and IR1–IR9. Average trabecular bone parameter values (BV/TV,

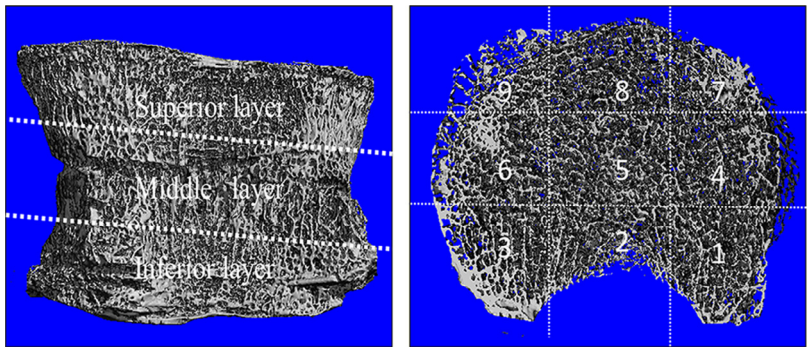

Fig. 4. Regional analysis of micro-computed tomography (micro-CT) imaging. (Left) Each vertebral body was divided into three layers (posterior on the right). (Right) Each layer was divided into nine regions (posterior at the bottom).

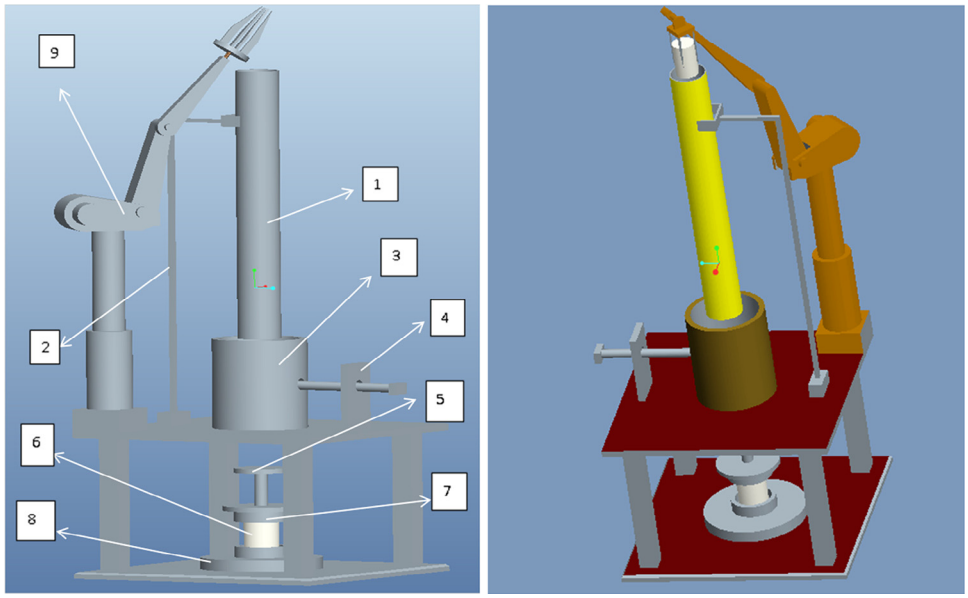

Fig. 5. Apparatus for obtaining burst fractures: (1) guide tube, (2) bracing piece, (3) cylindrical barrier block, (4) limiting rod, (5) susceptor, (6) vertebral specimen, (7) dental plaster cup, (8) base plate, (9) manipulator.

BMD, Tb.N, etc.) from all three layers were measured by the micro-CT system [22–24].

Mechanical testing

Specimens were thawed in a sealed environment to prevent drying and dehydration, which can affect mechanical properties. The upper and lower vertebral bodies of each three-vertebra specimen were secured in cups of dental plaster, keeping the L1 vertebral body in the horizontal position as far as possible. Specimens were mounted in our specially designed gravity impact machine (Fig. 5). After installation, the 5.0-kg hammer fell freely from a 1.4-m height and impacted the susceptor. The limiting rod was quickly pushed on the other side to prevent the weight dropping twice [25–30]. If necessary, the impact was repeated until a satisfactory burst fracture was obtained. Then CT scanning and three-dimensional reconstruction were used to observe the fracture and to obtain the parameters RL, RW, RH, VL, VW, and VH.

Specimen observation

Tested specimens were frozen at −20°C. Then the posterior column was removed at the pedicles so that we could observe the fracture and any longitudinal ligament rupture [31–33]. The intervertebral discs were bisected to obtain individual vertebral bodies, which were sectioned in the midsagittal plane so that we could observe the relationship between the fracture line and the BF.

Statistical analysis

Interobserver reliability of dimensional measurements was analyzed using the kappa statistic [34]. Numerical data, including RL, RW, RH, VL, VW, VH, were tested by the one-sample Kolmogorov-Smirnov test to determine if it was well-modeled by a normal distribution [35]. Average values, including BV/TV, SMI, Conn.D, Tb.N, Tb.Th, Tb.Sp, and BMD, were obtained for each region, and differences among the three spinal levels (T12, L1, and L2) were tested by one-way analysis of variance (ANOVA). Differences between the nine regions in each layer were also tested using one-way ANOVA and paired Student *t* test. We use two-way ANOVA to analyze the presence of interactions between layers and regions. Descriptive statistics, including standard deviations (SD) and confidence intervals, were calculated assuming normally distributed raw data. All analyses were performed with the SPSS 20.0 statistical package (SPSS Statistics for Windows, IBM Corp., Armonk, NY, USA). Statistical significance was defined as $p<.05$.

Results

CT sagittal reconstruction images suggested all fractures with an RBF were in the posterior margin of the vertebral body. Thirty-four patients had fracture lines, but with no obvious shift, and the other 128 patients with different degrees of shift and turnover. In 139 patients, the fracture lines of RBFs went across the vertex (or upper surface) of the BF and the RBF included all or part of the upper surface of the BF.

Dimensions of RBF and vertebrae

Kappa values averaged 0.709~0.816, indicating good interobserver reliability of measurements. Dimensions of the RBFs and vertebral bodies are given in Tables 1–3, together with various ratios: for example RL/VL is the ratio of the length of the RBF compared with the vertebral body. Values of RL/VL and RH/VH were 0.497±0.049 and 0.480±0.035, respectively, which means that RBFs were approximately half as long and as high as the vertebral body. Similarly, widths of RBFs were 0.314±0.021 and approximately one-third the width of the vertebral body. All data were approximately normal ($p>.05$) and did not vary significantly between T12, L1, and L2.

Micro-CT analysis

Indicators of trabecular bone quality, including BV/TV, Conn.D, Tb.N, Tb.Th, and BMD, were often lowest in the MR2, MR5, and SR5 regions, whereas SMI and Tb.Sp were often correspondingly higher (Tables 4 and 5). Many differences were statistically significant ($p<.05$) and, although p-values must be interpreted with caution because of multiple significance testing, the consistency of differences suggests that these three regions are often weak in the vertebral body. The BF is located in these areas, so it could become a potential risk of fracture. There were few significant differences between regions in the inferior layer. Two-way ANOVA results show that different layers and regions will influence the trabecular bone parameters, respectively, but the interaction effects between them were not significant.

Mechanical test verification

In these 12 specimens, three specimens had a compression fracture and the height of the vertebral body was decreased in the process of impact, which did not form typical of RBF and was identified as a simulation failure. In the remaining nine specimens, the burst fractures and RBFs were similar to the clinical cases, as intended (Fig. 6), so we successfully simulated burst fracture in nine specimens. Statistical analysis showed that the ratios of RL/VL, RW/VW, and RH/VH were not significantly different between clinical cases and the simulated RBFs ($p>.05$). In these nine specimens, the fracture line of RBF went across the vertex or the upper surface of BF, and the RBF includes all or part of the upper surface of the BF.

After removal of the posterior column, three specimens showed no obvious posterior longitudinal ligament (PLL) damage, and the other six had different degrees of PLL

Table 1
Length of the retropulsed bone fragments and vertebral body

	N	RL	VL	RL/VL	95% Confidence intervals
T12	18	21.20±2.775	43.40±4.037	0.488±0.042	0.436~0.540
L1	32	20.25±2.563	41.50±4.034	0.501±0.055	0.466~0.536
L2	24	21.60±2.881	43.60±5.506	0.496±0.046	0.438~0.553
Total	74	21.05±2.572	42.41±4.067	0.497±0.049	0.475~0.518

RL, length of the retropulsed bone fragments; VL, length of vertebral body; RW, width of retropulsed bone fragments; VW, width of vertebral body.
Notes: Values are mean±SD in mm. 95% Confidence intervals refer to the ratio RW/VW.

Table 2
Width of the retropulsed bone fragments and vertebral body

	N	RW	VW	RW/VW	95% Confidence intervals
T12	18	9.20±1.924	28.80±3.633	0.317±0.034	0.276~0.359
L1	32	9.67±1.497	30.75±4.159	0.314±0.022	0.300~0.328
L2	24	10.0±1.581	32.40±2.302	0.308±0.040	0.257~0.358
Total	74	9.64±1.560	30.68±3.759	0.314±0.021	0.301~0.326

RW, width of the retropulsed bone fragments; VW, width of vertebral body; RW, width of retropulsed bone fragments; VW, width of vertebral body.
Notes: Values are mean±SD in mm. 95% Confidence intervals refer to the ratio RW/VW.

Table 3
Height of the retropulsed bone fragments and vertebral body

	N	RH	VH	RH/VH	95% Confidence intervals
T12	18	12.20±2.168	23.8±3.962	0.512±0.034	0.470~0.554
L1	32	10.17±1.467	21.5±2.335	0.472±0.034	0.450~0.493
L2	24	11.00±1.414	23.6±2.408	0.465±0.020	0.440~0.490
Total	74	10.82±1.763	22.5±2.874	0.480±0.035	0.464~0.495

RH, height of the retropulsed bone fragments; VH, height of vertebral body.
Notes: Values are mean±SD in mm. 95% Confidence intervals refer to the ratio RH/VH.

Table 4
Trabecular parameters for each region in the middle layer

Parameter	Region	MR1	MR2	MR3	MR4	MR5	MR6	MR7	MR8	MR9
BV/TV	Value	0.40±0.06	0.34±0.07	0.39±0.03	0.37±0.06	0.33±0.06	0.36±0.06	0.39±0.07	0.33±0.05	0.38±0.06
	MR2	**p=.010***	/	**p=.030***	**p=.023***	p=.667	**p=.004***	**p=.039***	p=.395	**p=.028***
	MR5	**p=.025***	p=.667	**p=.012***	**p=.011***	/	**p=.036***	**p=.041***	p=.186	p=.678
SMI	Value	0.19±0.55	0.58±0.50	0.10±0.38	0.33±0.48	0.72±0.43	0.37±0.46	0.04±0.52	0.43±0.50	0.19±0.55
	MR2	**p=.025***	/	**p=.016***	**p=.005***	p=.824	p=.398	**p=.006***	p=.582	**p=.028***
	MR5	**p=.030***	p=.824	**p=.001***	**p=.007***	/	**p=.006***	**p=.023***	**p=.023***	**p=.021***
Tb.N (1/mm)	Value	1.44±0.25	1.18±0.27	1.35±0.12	1.35±0.30	1.23±0.25	1.33±0.29	1.31±0.34	1.08±0.20	1.44±0.25
	MR2	**p=.018***	/	**p=.008***	**p=.007***	p=.952	**p=.006***	**p=.014***	p=.675	**p=.0002***
	MR5	**p=.043***	p=.952	**p=.021***	**p=.002***	/	**p=.013***	**p=.021***	p=.878	**p=.010***
BMD (mgHA/cm^3)	Value	442.54±50.00	453.99±69.31	439.08±46.88	418.09±56.07	447.95±79.44	442.54±50.00	453.99±69.31	439.08±46.88	418.09±56.07
	MR2	**p=.043***	/	**p=.049***	**p=.016***	**p=.010***	**p=.047***	**p=.038***	**p=.018***	**p=.004***
	MR5	p=.330	**p=.010***	p=.647	**p=.023***	/	p=.890	**p=.037***	p=.552	**p=.017***

BV/TV, bone volume/trabecular volume; SMI, structure model index; Tb.N, number of trabecular; BMD, bone mineral density; MR, middle region.
Note: Values are mean±SD.
* Bold indicates significant differences (p<.05). Data suggest that the MR2 and MR5 regions are often weaker than adjacent regions.

Table 5
Trabecular parameters for each region in the superior layer

Parameter	Region	SR1	SR2	SR3	SR4	SR5	SR6	SR7	SR8	SR9
BV/TV	Value	0.43±0.05	0.40±0.07	0.44±0.04	0.43±0.06	0.36±0.09	0.41±0.04	0.47±0.06	0.43±0.07	0.43±0.05
	SR2	**p=.003***	/	p=.694	**p=.040***	p=.818	p=.853	**p=.033***	p=.933	p=.798
	SR5	**p=.017***	p=.818	**p=.020***	**p=.016***	/	p=.533	**p=.032***	**p=.027***	**p=.046**
SMI	Value	−0.21±0.61	0.07±0.49	−0.33±0.48	−0.12±0.74	0.41±0.75	0.04±0.48	−0.70±0.78	−0.29±0.78	−0.87±0.57
	SR2	p=.051	/	**p=.032***	p=.802	p=.153	p=.183	p=.356	**p=.027***	**p=.031***
	SR5	p=.622	p=.153	p=.146	**p=.046***	/	p=.278	**p=.021***	**p=.029***	**p=.014***
Tb.N (1/mm)	Value	1.49±0.21	1.41±0.36	1.46±0.11	1.52±0.18	1.29±0.40	1.48±0.14	1.52±0.23	1.35±0.30	1.49±0.21
	SR2	p=.139	/	p=.615	p=.739	**p=.009***	p=.275	p=.503	p=.569	p=.082
	SR5	p=.234	**p=.009***	p=.841	**p=.021***	/	p=.710	**p=.005***	p=.115	p=.303
BMD (mgHA/cm^3)	Value	422.91±47.22	456.08±58.84	430.64±43.28	417.54±42.43	435.48±57.45	417.58±35.51	411.17±52.98	426.03±71.73	422.91±47.22
	SR2	**p=.017***	/	p=.377	**p=.019***	p=.141	**p=.026***	p=.803	p=.234	**p=.023***
	SR5	p=.274	p=.141	p=.056	**p=.016***	/	**p=.004***	p=.444	p=.761	p=.728

BV/TV, bone volume/trabecular volume; SMI, structure model index. Tb.N, number of trabecular; BMD, bone mineral density. SR, superior region.
Note: Values are mean±SD.
* Bold indicates significant differences (p<.05). Data suggest that the SR2 and SR5 regions have the tendency to be weaker than adjacent regions, although it does not often reach statistical significance.

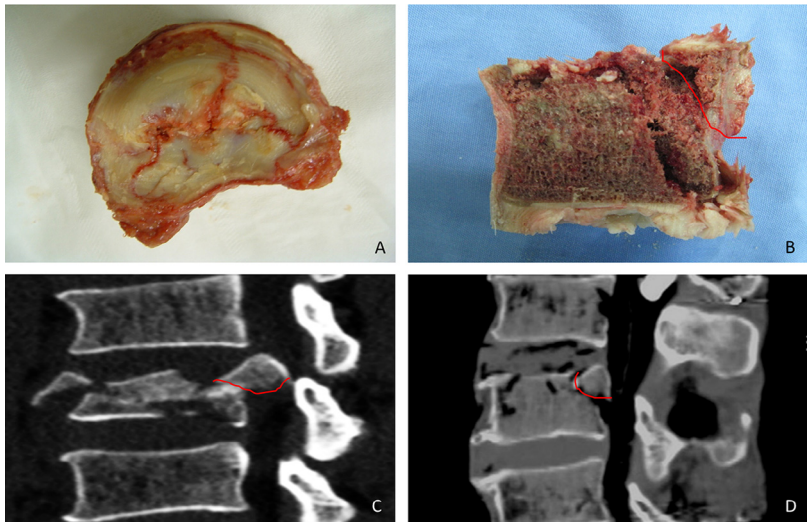

Fig. 6. Burst fractures simulated in our specially designed gravity impact machine. (A) Gross morphology of superior end plate fracture. The fracture line was located near region SR2. (B) Gross morphology of RBF in sagittal plane. (C) Sagittal CT image of a simulated comminuted fracture. Note the loss of vertebral body height. (D) Sagittal CT image of simulated burst fracture, showing a typical RBF which was consistent with our objective. The RBF was pointed out in red curve. CT, computed tomography; RBF, retropulsed bone fragment; SR2, superior region 2.

damage. The damage sites were mainly located on the edge of the BF. When we removed the PLL to reveal the posterior margin of the vertebral body, the RBF appeared to be similar to the clinical imaging findings. After adjacent vertebral bodies were separated through the intervertebral disc, seven specimens had different degrees of upper end plate injury, and two specimens had lower end plate injury. Then along the median sagittal, we sectioned the vertebral body longitudinally, and found the fracture line of RBF went across the vertex or the upper surface of BF (Fig. 6).

Relationship of RBF to the basivertebral foramen

Fractures were often located in the one-third posterior upper regions of the vertebral body, equivalent to the SR2 area which is located just superior to the BF. The fracture line of RBF went across the vertex (or upper surface) of the BF and the RBF included all or part of it (Fig. 6).

Discussion

Our study shows that many RBFs are located around the BF and often include all or part of it, suggesting that the BF may contribute to the formation of a burst fracture. RBF dimensions ranged from one-third to half of the vertebral body dimensions, and their location was adjacent to the BF (often within the SR2 region), suggesting a causal link. Micro-CT scanning showed inferior trabecular microstructure in the MR2, MR5, and SR5 regions, suggesting a weakening effect of the BF. These weak areas can result in RBF following vertical energy. Simulated burst fractures on cadaveric spines showed similar RBFs to those seen in clinical cases, with close approximation to the BF in the SR2 region, emphasizing that RBF formation is closely associated with the BF.

Close spatial association between the BF and the RBF has been reported previously, with the RBF extending from the upper end plate to the upper surface of the BF [7]. This would imply that RH/VH should be close to one-half, rather than one-third as reported here. Possibly, shear stress transfers into the vertebral body along the pedicle, and forms a stress concentration zone in the medial pedicle as well as in the MR2 region [13,15,16], so the value of RL/VL is bigger than one-third.

Combining the present results with previous literature suggests that the mechanism of RBF formation may be as follows. Rapid vertical loading increases intervertebral disc pressure and makes an end plate rupture. Nucleus pulposus is squeezed into the vertebral body, resulting in a high internal (intravertebral) pressure which causes the vertebral cortex to burst [1]. The SR5 and SR2 regions have a more vulnerable trabecular network than other regions in the superior layer (Table 5), and the superior layer has been shown to be weaker than the inferior layer [17] so vertical load causes SR5 and SR2 to fracture first. Vertebral height loss increases neural arch load-bearing [36] and impacted neural arches create additional shear stresses to be transferred from the pedicles, leading to fracture in the vulnerable middle layer of the vertebral body, in the region of the BF. Finally, a fracture block is formed in which the upper vertebral end plate is the upper bound, the cut stress transmission surface of the pedicles form the left and right boundaries, and the lower bound is all or part upper surface of the BF [13,15–17].

We suggest that our paper is the first large clinical study to combine clinical, mechanical, and bone quality measurements to explain the exact location and origins of RBFs. We

show that the BF influences local trabecular strength and hence the boundaries of RBFs. Previous studies have only found the upper boundary and left and right boundary of RBFs, whereas our study has found the anterior and lower boundaries of RBF are also determined by the BF.

These findings have several clinical implications. The location and size of the fracture block are important for the identification and treatment of thoracolumbar burst fractures. The present study suggests that the displaced fracture block is a marker for posterior longitudinal ligament rupture, and simple posterior pedicle screw retraction reduction cannot obtain fully decompression and reduction [37,38]. The fracture block shifts backward and compresses the spinal cord, which leads to spinal stenosis, nerve function injury, and paraplegia. In this circumstance, surgery is necessary to remove the compression fracture block to reduce spinal cord injury [10,27,39–43]. What's more, if the upper edge of bone fragments into the spinal canal is more than 50%–75% canal area, anterior decompression is required [42,43]. Therefore, it is helpful to evaluate the damage of posterior longitudinal ligament and spinal cord injury, which is an important basis for the selection of a surgical approach and the implementation of the operation. During preoperative evaluation, we should possibly consider whether the BF structure is intact, and when we perform distraction reduction, we should try to avoid damage to the BF. We speculate that an incomplete BF could interfere with blood vessels in a manner that might influence bone healing. When we use polymethyl methacrylate (PMMA) filling in vertebrae to strengthen the effect of internal fixation, we also should consider the BF structure which may be a potential risk factor for cement leakage through it if it is connected with the intravertebral cleft [44]. Our study confirms the relationship of BF and RBF so as to further explore the inherent relationship and clinical significance to guide our surgeries in our later research.

In young specimens that have no intervertebral disc degeneration, a rapid vertical load concentrates stress in the posterior margin of the vertebral body and it is easy to produce a burst fracture. However, in old specimens with intervertebral disc degeneration, it is easier to produce end plate ("compressive") fracture [23,45–47], and the addition of flexion then leads to "anterior wedge" fractures [48]. We aimed to use young specimens as far as possible in these mechanical tests, but they are difficult to obtain so it was necessary to include several relatively old cadaveric spines.

This study has several limitations. Multiple significance testing between mean values in Tables 1–5 could yield some spurious results. However, this problem can be minimized if the reader makes direct comparisons between specific mean values of interest, using their 95% confidence intervals to determine significance. Our mechanical study did not consider different injury mechanisms (such as traffic accidents and falls from height) that could lead to different fracture patterns such as sagittal split or asymmetric split [49], and specimen weight, height, and BMD were not considered.

Conclusions

The BF, a vertebral bone default zone, is the most unsubstantial region in the vertebral body which influences the distribution of trabeculae around it. Vertical energy applied to relatively young spines leads to failure under the superior end plate, which then spreads to the region of the BF, with the formation of a burst fracture including an RBF.

Acknowledgments

This study was partially supported by the National Natural Science Foundation of China (No. 31270997 and No. 81672208). The authors thank Prof. Michael Adams and Prof. Trish Dolan for their assistance with the manuscript.

References

[1] Langrana NA, Harten RR, Lin DC, Reiter MF, Lee CK. Acute thoracolumbar burst fractures: a new view of loading mechanisms. Spine 2002;27:498–508.
[2] Wang XY, Dai LY, Xu HZ, Chi YL. Biomechanical effect of the extent of vertebral body fracture on the thoracolumbar spine with pedicle screw fixation: an in vitro study. J Clin Neurosci 2008;15:286–90.
[3] Khoueir P, Oh BC, Wang MY. Delayed posttraumatic thoracolumbar spinal deformities: diagnosis and management. Neurosurgery 2008;63(Suppl. 3):117–24.
[4] Kifune M, Panjabi MM, Arand M, Liu W. Fracture pattern and instability of thoracolumbar injuries. Eur Spine J 1995;4:98–103.
[5] Dai LY, Wang XY, Jiang LS. Neurologic recovery from thoracolumbar burst fractures: is it predicted by the amount of initial canal encroachment and kyphotic deformity? Surg Neurol 2007;67:232–7 discussion 8.
[6] Kim NH, Lee HM, Chun IM. Neurologic injury and recovery in patients with burst fracture of the thoracolumbar spine. Spine 1999;24:290–3 discussion 4.
[7] Guerra J Jr, Garfin SR, Resnick D. Vertebral burst fractures: CT analysis of the retropulsed fragment. Radiology 1984;153:769–72.
[8] DeVivo MJ. Causes and costs of spinal cord injury in the United States. J Urol 1998;2308.
[9] Meves R, Avanzi O. Correlation among canal compromise, neurologic deficit, and injury severity in thoracolumbar burst fractures. Spine 2006;31:2137–41.
[10] Eberl R, Kaminski A, Muller EJ, Muhr G. Importance of the cross-sectional area of the spinal canal in thoracolumbar and lumbar fractures. Is there any correlation between the degree of stenosis and neurological deficit? Orthopade 2003;32:859–64.
[11] McCormack T, Karaikovic E, Gaines RW. The load sharing classification of spine fractures. Spine 1994;19:1741–4.
[12] Hongo M, Abe E, Shimada Y, Murai H, Ishikawa N, Sato K. Surface strain distribution on thoracic and lumbar vertebrae under axial compression. The role in burst fractures. Spine 1999;24:1197–202.
[13] Qiu TX, Tan KW, Lee VS, Teo EC. Investigation of thoracolumbar T12-L1 burst fracture mechanism using finite element method. Med Eng Phys 2006;28:656–64.
[14] Grant JP, Oxland TR, Dvorak MF. Mapping the structural properties of the lumbosacral vertebral endplates. Spine 2001;26:889–96.
[15] Heggeness MH, Doherty BJ. The trabecular anatomy of thoracolumbar vertebrae: implications for burst fractures. J Anat 1997;191(pt 2):309–12.
[16] Overaker DW, Langrana NA, Cuitino AM. Finite element analysis of vertebral body mechanics with a nonlinear microstructural model for the trabecular core. J Biomech Eng 1999;121:542–50.
[17] Zhao FD, Pollintine P, Hole BD, Adams MA, Dolan P. Vertebral fractures usually affect the cranial endplate because it is thinner and supported by less-dense trabecular bone. Bone 2009;44:372–9.

[18] O'Connor SD, Yao J, Summers RM. Lytic metastases in thoracolumbar spine: computer-aided detection at CT—preliminary study. Radiology 2007;242:811–16.
[19] Crock HV, Yoshizawa H, Kame SK. Observations on the venous drainage of the human vertebral body. J Bone Joint Surg Br 1973; 55:528–33.
[20] Panjabi MM, Krag M, Summers D, Videman T. Biomechanical time-tolerance of fresh cadaveric human spine specimens. J Orthop Res 1985;3:292–300.
[21] Bouxsein ML, Boyd SK, Christiansen BA, Guldberg RE, Jepsen KJ, Muller R. Guidelines for assessment of bone microstructure in rodents using micro-computed tomography. J Bone Miner Res 2010;25:1468–86.
[22] Hulme PA, Boyd SK, Ferguson SJ. Regional variation in vertebral bone morphology and its contribution to vertebral fracture strength. Bone 2007;41:946–57.
[23] Gong H, Zhang M, Yeung HY, Qin L. Regional variations in microstructural properties of vertebral trabeculae with aging. J Bone Miner Metab 2005;23:174–80.
[24] Baker ADL. The three column spine and its significance in the classification of acute thoracolumbar spinal injuries. 2014. p. 289–92.
[25] Panjabi MM, Hoffman H, Kato Y, Cholewicki J. Superiority of incremental trauma approach in experimental burst fracture studies. Clin Biomech (Bristol, Avon) 2000;15:73–8.
[26] Panjabi MM, Kifune M, Liu W, Arand M, Vasavada A, Oxland TR. Graded thoracolumbar spinal injuries: development of multidirectional instability. Eur Spine J 1998;7:332–9.
[27] Panjabi MM, Kifune M, Wen L, et al. Dynamic canal encroachment during thoracolumbar burst fractures. J Spinal Disord 1995;8:39–48.
[28] Jones HL, Crawley AL, Noble PC, Schoenfeld AJ, Weiner BK. A novel method for the reproducible production of thoracolumbar burst fractures in human cadaveric specimens. Spine J 2011;11:447–51.
[29] Kallemeier PM, Beaubien BP, Buttermann GR, Polga DJ, Wood KB. In vitro analysis of anterior and posterior fixation in an experimental unstable burst fracture model. J Spinal Disord Tech 2008;21:216–24.
[30] Borkowski SL, Sangiorgio SN, Bowen RE, Scaduto AA, Kwak J, Ebramzadeh E. Flexibility of thoracic spines under simultaneous multi-planar loading. Eur Spine J 2014;doi:10.1007/s00586-014-3499-0.
[31] Ghole SA, Ivancic PC, Tominaga Y, Gimenez SE, Panjabi MM. Incremental and single trauma produce equivalent subfailure soft tissue injury of the cervical spine. Clin Biomech (Bristol, Avon) 2004;19:784–9.
[32] Wiltse LL, Fonseca AS, Amster J, Dimartino P, Ravessoud FA. Relationship of the dura, Hofmann's ligaments, Batson's plexus, and a fibrovascular membrane lying on the posterior surface of the vertebral bodies and attaching to the deep layer of the posterior longitudinal ligament. An anatomical, radiologic, and clinical study. Spine 1993;18:1030–43.
[33] Verlaan JJ, van de Kraats EB, Oner FC, van Walsum T, Niessen WJ, Dhert WJ. Bone displacement and the role of longitudinal ligaments during balloon vertebroplasty in traumatic thoracolumbar fractures. Spine 2005;30:1832–9.
[34] Kottner J, Audige L, Brorson S, et al. Guidelines for reporting reliability and agreement studies (GRRAS) were proposed. Int J Nurs Stud 2011;48:661–71.
[35] Hazra A, Gogtay N. Biostatistics series module 3: comparing groups: numerical variables. Indian J Dermatol 2016;61:251–60.
[36] Luo J, Skrzypiec DM, Pollintine P, Adams MA, Annesley-Williams DJ, Dolan P. Mechanical efficacy of vertebroplasty: influence of cement type, BMD, fracture severity, and disc degeneration. Bone 2007; 40:1110–19.
[37] Leferink VJ, Nijboer JM, Zimmerman KW, Veldhuis EF, ten Vergert EM, ten Duis HJ. Burst fractures of the thoracolumbar spine: changes of the spinal canal during operative treatment and follow-up. Eur Spine J 2003;12:255–60.
[38] Boerger TO, Limb D, Dickson RA. Does "canal clearance" affect neurological outcome after thoracolumbar burst fractures? J Bone Joint Surg Br 2000;82:629–35.
[39] Dai LY, Wang XY, Jiang LS. Evaluation of traumatic spinal canal stenosis in thoracolumbar burst fractures. A comparison of three methods for measuring the percent canal occlusion. Eur J Radiol 2008;67:526–30.
[40] Shen WJ, Liu TJ, Shen YS. Nonoperative treatment versus posterior fixation for thoracolumbar junction burst fractures without neurologic deficit. Spine 2001;26:1038–45.
[41] Mikles MR, Stchur RP, Graziano GP. Posterior instrumentation for thoracolumbar fractures. J Am Acad Orthop Surg 2004;12:424–35.
[42] Zhu Q, Shi F, Cai W, Bai J, Fan J, Yang H. Comparison of anterior versus posterior approach in the treatment of thoracolumbar fractures: a systematic review. Int Surg 2015;100:1124–33.
[43] Tezer M, Ozturk C, Aydogan M, Mirzanli C, Talu U, Hamzaoglu A. Surgical outcome of thoracolumbar burst fractures with flexion-distraction injury of the posterior elements. Int Orthop 2005;29:347–50.
[44] Wang C, Fan S, Liu J, Suyou L, Shan Z, Zhao F. Basivertebral foramen could be connected with intravertebral cleft: a potential risk factor of cement leakage in percutaneous kyphoplasty. Spine J 2014;14:1551–8.
[45] Shirado O, Kaneda K, Tadano S, Ishikawa H, McAfee PC, Warden KE. Influence of disc degeneration on mechanism of thoracolumbar burst fractures. Spine 1992;17:286–92.
[46] Jung JY, Lee MH, Ahn JM. Leakage of polymethylmethacrylate in percutaneous vertebroplasty: comparison of osteoporotic vertebral compression fractures with and without an intravertebral vacuum cleft. J Comput Assist Tomogr 2006;30:501–6.
[47] Sarli M, Perez Manghi FC, Gallo R, Zanchetta JR. The vacuum cleft sign: an uncommon radiological sign. Osteoporos Int 2005;16:1210–14.
[48] Adams MA, Pollintine P, Tobias JH, Wakley GK, Dolan P. Intervertebral disc degeneration can predispose to anterior vertebral fractures in the thoracolumbar spine. J Bone Miner Res 2006;21:1409–16.
[49] Atlas SW, Regenbogen V, Rogers LF, Kim KS. The radiographic characterization of burst fractures of the spine. AJR Am J Roentgenol 1986;147:575–82.